JOURNAL OF Applied Polymer SCIENCE

Facile Fabrication of Polyimide Foam Sheets with Millimeter Thickness: Processing, Morphology, and Properties

Jing-Jing Ma, Mao-Sheng Zhan, Kai Wang
School of Material Science and Engineering, Beijing University of Aeronautics and Astronautics, Beijing 100191, People's Republic of China
Correspondence to: M.-S. Zhan (E-mail: zhanms@buaa.edu.cn) or J.-J. Ma (E-mail: majingjingbh@126.com)

ABSTRACT: A series of polyimide foam sheets (PIFSs) with thickness of 0.5 mm using 3,3′,4,4′-benzophenonetetracarboxylic dianhydride (BTDA), 3,4′-oxydianiline (3,4′-ODA), and polyaryl polymethylene isocyanate (PAPI) as main materials were first fabricated by liquid foaming and compression molding technology. The effects of different PAPI contents and 3,4′-ODA contents on the structures and properties of PIFSs were investigated. The results indicated that PIFSs exhibited a structure that front surface displayed closed cells made of damaged cell walls and membranes, while internal cells were open, and elliptic vacancies were flatted in the thickness direction from the cross section. The average cellular diameter increased with increasing PAPI loading. In addition, the introduction of 3,4′-ODA increased the average cell size of PIFSs. Further, PIFSs had density of 0.087–0.239 g/cm^3, elongation at break of 3.75–8.01% and tensile toughness of 3.46×10^{-2}–13.87×10^{-2} J/cm^3. Notably, they exhibited higher tensile strength of 1.89–5.42 MPa and lower thermal conductivity of 14.727–19.25 mW/m •K at 24°C, compared to the polyimide foams reported earlier. The sound absorption coefficients (α) of samples with different PAPI contents increased and then decreased with increasing PAPI content. At low frequencies, a certain content of 3,4′- ODA allowed an improvement of the acoustical behavior of PIFSs, and the α increased and then decreased with increasing density. © 2013 Wiley Periodicals, Inc. J. Appl. Polym. Sci. **2014**, *131*, 39881.

KEYWORDS: structure–property relations; porous materials; polyimides; morphology; foams

Received 18 May 2013; accepted 24 August 2013
DOI: 10.1002/app.39881

INTRODUCTION

Foam sheet is an important class of planar materials with thickness of 0.1–5 mm composed of continuous solid polymer and gaseous cells dispersed throughout the solid.[1] Due to light weight, low thickness, porosity, and sound insulation, they are of interest for many applications including industry, building, medicine, packaging, and so on.[2] Although conventional foam sheets such as polyethylene foamed sheet (EPE),[2] polystyrene foam,[3,4] poly (methyl methacrylate) foam,[5] polyurethane foam[6,7] are mostly studied, potential applications of them in aerospace, industry, and daily life have been restricted because of their inflammability, poor thermal insulation and poor high-temperature stability. For many aerospace applications, such as multilayer insulation (MLI) blankets of BepiColombo,[8] it is most desirable to have higher temperature stability, flexibility, low thermal conductivity. Further, as the aerospace systems mostly need to occupy small space, minimizing the weight and thickness of the system as well as providing excellent performance must be taken into consideration.

PIFSs are novel materials developed in recent years. They have a number of attractive functional attributes such as light weight, low thickness, porosity, thermal insulation, sound insulation, low smoke generation, radiation resistance, and fire resistance,[9–11] making them to be one kind of ideal materials for aerospace and applications including thermal insulation and high temperature. For instance, Aerofoam PIF 4–6_1000[8,12] with 1 mm thickness has been used in high-temperature multilayer insulation (HT-MLI) of BepiColombo as blankets. It is yellow-colored transparent polyimide foam with a density of 0.004–0.006 g/cm^3. And it possesses tensile stress of 0.1 MPa, thermal conductivity of 35 mW/(m•K) and high temperature stability. BF301 and BP101 previously reported by the UBE[13,14] are candidates ever for MLI, and they possess thickness of 2 mm, low thermal conductivity of 35–54 mW/(m•K), density of 0.023–0.270 g/cm^3 and porosity up to 97.9%. Polyimide aerogel thin films[15–18] with high porosity are flexible and are produced at densities of 0.108–0.451 g/cm^3. As a consequence of low density, low thickness of 0.5 mm and low thermal conductivity of 14 mW/(m•K), they are potentially used in aerospace applications for entry, descent, and landing operations.[19] Dustin Miller et al.[20,21] fabricated microcellular and nanocellular polyetherimide (PEI) foam sheets with thickness of 1–2 mm which

possessed high strength stress of 66–93 MPa. However, they exhibited bad flexibility and high density of 0.96–1.128 g/cm^3.

Although PIFSs are widely studied, their developments have been restricted because of their inefficient processing methods. For instance, these PIFSs such as BP101, BP011, and BP021 developed on the basis of powdered precursor process[22–24] are relatively expensive to produce because of their long production cycle, complex technology, toxicity of methanol as solvent, and expensive mold equipment. Another common process to fabricate PIFSs is super-critical CO_2 process which has time-consuming nature.[15–18,20,21] For example, the saturation time of PEI sheets with thickness of 1.5 mm using CO_2 was about 350 h at 5MPa and one small-size sample was obtained once due to the expensive and complex equipment. As a result, it is challenging to prepare an ultrathin PIFS with good properties by a low-cost process which is simple and has short production cycle. Further, due to the large variation in thickness resulting in variation in cell structure and the difficulty in obtaining foam sheets of millimeter thickness, it remains a big challenge that the research on the effects of composition on structure and performance of PIFSs.

The object of this work is to use a facile and effective method to fabricate PIFSs with cells and good properties of low density, high tensile strength, low thermal conductivity and high sound absorption coefficient. In this article, a series of PIFSs using BTDA, 3,4′-ODA and PAPI as main materials were first successfully fabricated by liquid foaming and compression molding technology which have the advantage over other technology of short molding cycle resulting in lower cost and faster production rates. The relationships among compositions, structures, and properties of PIFSs, including cell morphologies, apparent densities, mechanical properties, thermal insulation properties, sound absorption properties, and so forth, were discussed. The test data can also demonstrate that the well-defined properties potentially make the lightweight PIFSs with millimeter thickness to be candidates for MLI of spacecrafts and other applications.

EXPERIMENTAL

Materials

BTDA was acquired from Beijing Multi Technology Co. Ltd., China, and was dried in a vacuum oven at 150°C for 8–10 h before use. PAPI (PM-200) was obtained from Yantai Wanhua Polyurethanes Co. Ltd., China. 3,4′-ODA was purchased from Shanghai Research Institute of Synthetic Resins, China, and it must be purified before use. Silicone oil (DC-193) was purchased from Foshan Daoning Chemical Co. Ltd., China, and it was the main surfactant. Polyethylene glycol 600 (PEG-600), N, N′-dimethylformamide (DMF), methanol, and deionized water were all supplied by Beijing Finechem, China.

Preparation

Preparation of PIFSs based on BTDA and PAPI. A series of 0.5 mm PIFSs with different weight ratios of PAPI to first solution were prepared by two steps composed of liquid foaming and compression molding. First, foam intermediates were prepared as our previous report.[25] BTDA, DMF, methanol, demonized water, DC-193, and PEG-600 were accurately weighted and added to a 250 ml-volume flask at approximately 85°C. The mixture was stirred for 2 h to give a homogeneous solution named as first solution. When the first solution was cooled to 25°C, PAPI was added to the first solution. The combination of first solution and PAPI was stirred with a high speed mixer (about 2000 rpm) for 5–15 s. Then it was immediately transferred to a mould where it was allowed to rise freely for 4 min. Once the foam was no longer tacky, it was then transferred to a microwave oven at 30 W for 10 min to produce intermediate foam. Second, intermediate foam was rapidly transferred to a mold cavity that was connected with hot plates whose temperatures were 200°C. After the filling, the intermediate foams were subjected to compressing molding with pressure of 13.28–19.76 KPa for 2 h until the completion of imidization to give a 0.5 mm polyimide foam sheet. The weight ratios of PAPI to first solution for PIFSs prepared were from 0.5, 0.65, 0.8, 0.95, to 1.1. They were identified as PIFS-1, PIFS-2, PIFS-3, PIFS-4, and PIFS-5, respectively. According to the composition of PIFS-3, a series of PIFSs varying in density were fabricated by varying molding pressure from 13.28 KPa, 18.23 KPa, to 19.76 KPa. And they were designated as PIFS-3-1′, PIFS-3-2′, and PIFS-3-3′, respectively. The chemical reaction which might occur during the preparation was shown in Scheme 1.

Preparation of PIFSs based on BTDA, 3,4′-ODA and PAPI. A series of 0.5 mm PIFSs with different mole ratios of 3,4′-ODA to BTDA were prepared by three steps made of synthesis of polyamide acid, liquid foaming and compression molding. First, polyamide acid was synthesized using BTDA and 3,4′-ODA according to our previous technology.[26] Equimolar 3,4′-ODA and BTDA were accurately weighed and dissolved in DMF at room temperature. The mixture was stirred for 5 h until they completely reacted to get polyamide acid. Then, the remaining BTDA, DMF, methanol, water, DC-193 and PEG-600 were accurately weighted and added to it. The mixture was stirred for 2 h at 85°C to give first solution. Then PIFSs were prepared by the technology described above. These samples were expressed as PIFS-3-1, PIFS-3-2, PIFS-3-3, and PIFS-3–4 with 0.8 weight ratio of PAPI to first solution, whose mole ratios of 3,4′-ODA to BTDA were 5:100, 10:100, 15:100, and 20:100, respectively. According to the combination of PIFS-3–4, a series of foam sheets with thickness of 0.5 mm varying in density were fabricated by changing the molding pressure. They were designated as P1, P2, and P3, respectively. The chemical reaction which might occur during the preparation was presented in Scheme 2.

The resulting foamed product is yellow-colored PIFS with thickness of 0.5 mm, which is far thinner than the foam produced previously.[25,26] Further, they are flexible enough to bend back nearly 180°without cracking or flaking. Optical images of the foam sheets from different angles are presented in Figure 1.

Characterizations

The cell morphologies of samples were observed by a CS-3400 scanning electron microscopy (SEM). The specimens were sputter-coated with gold before testing. Their average cellular diameters were determined by SISAC-IAS image analyzer from the SEM images, and apparent density was tested according to ASTM D328. At least five samples were repeated for each test,

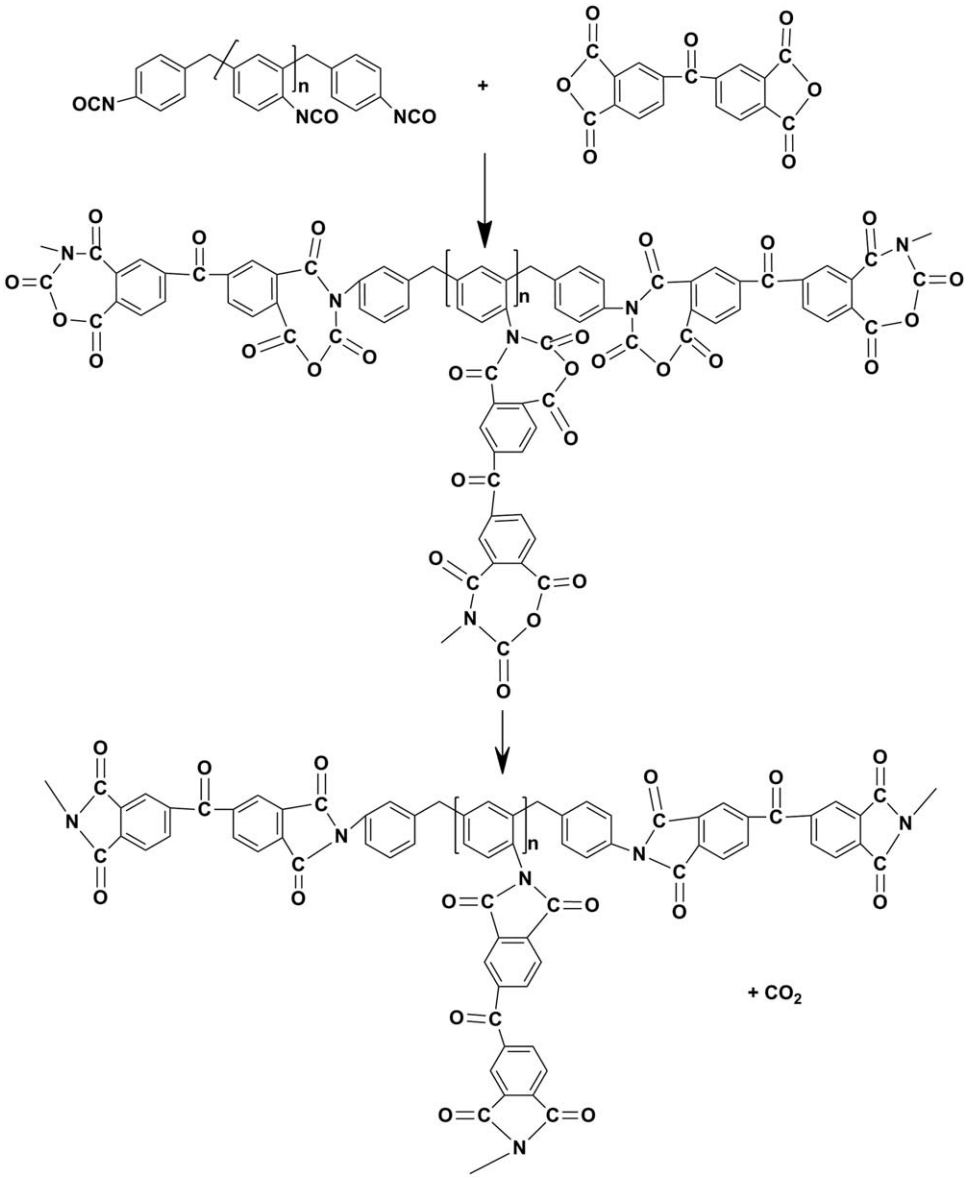

Scheme 1. The reaction during the preparation of PIFSs without 3,4′-ODA.

and the average value was used as the final result. Tensile properties investigation was carried out on an Instron5565 according to ASTM D638 and ASTM D882. The tensile specimens were cut into dumbbell bars with a dimension of 70 × 6 mm^2. A constant crosshead rate of 1 mm/min was carried while testing samples. Five samples were tested for each composition and results are given as averages with standard deviations. Thermal conductivity tests were measured on a thermal conductivity analyzer designed by ourselves previously according to ASTM C 518. The width and length of samples were all 50 mm. For each condition, five samples were tested to obtain the average data. The sound absorption coefficients at room temperature were monitored by a standing wave tube according to ISO-10534-2. The specimens were cut into rounded samples with 100 mm diameter and ten samples for each composition were tested in a BK-4206 impedance tube, to get average absorption coefficients. In this approach, the samples were placed at the impedance tube being backed by the rigid base board of the tube, and the thickness of the air-gap between the foam sheet and the rigid base board is zero.

RESULTS AND DISCUSSTION

Cell Structure Characterization of PIFSs

Representative samples with different weight ratios of PAPI to first solution were imaged by SEM with enlargement of 30 times to characterize the cell structures. Table I shows the cell sizes of PIFSs. SEM images of the samples are shown in Figure 2. As seen in Figure 2, PIFSs display closed cells made of damaged cell membranes and cell walls that were in the same plane, which is unlike the flexible foams produced earlier with open cells.[25] This could be explained in the following way: cell walls and membranes were damaged by molding pressure, generating the collapsing cells, thus compression opened the cell membranes and buckled the cell struts. PIFS-1 exhibits a structure

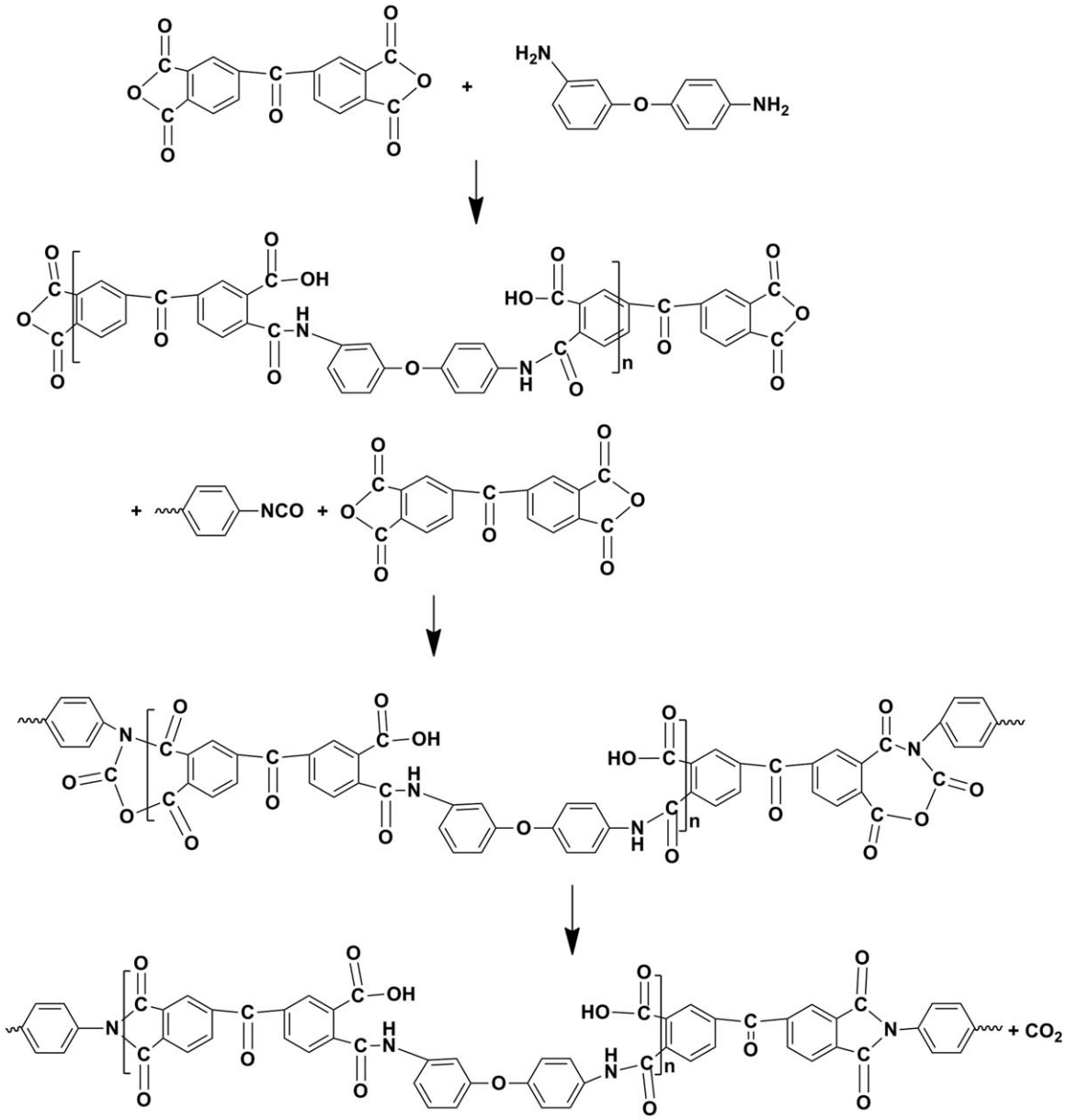

Scheme 2. The reaction during the preparation of PIFSs with 3,4′-ODA.

where clear areas of solid resin exist with rare cells. PIFS-2–PIFS-4 all present obvious cells that are characterized as sharing cellular walls. Further, their cells are flat like fishing net. While in PIFS-5, the cells are in a mess, and cell walls are difficult to find. Comprehensive analysis shows that the average cellular diameter increases from 100.42 μm to 339.07 μm with increasing PAPI loading. In this case, the uniformity of cellular size distribution increases firstly, and then reduces. This could be attributed to the varying released amount of gases. Equal quantities of first solutions were used for PIFS-1–PIFS-5; hence, the amount of reactive groups which generated CO_2 with PAPI was equal. So the reaction of first solution and PAPI are more rapid and the released amount of CO_2 increased with increasing PAPI contents, resulting in the larger cellular diameter and thinner cell walls. In PIFS-3, the amount of isocynate group is approximately equal to the amount of reactive groups, thus the reaction is the most complete, leading to relatively uniform cell size distribution. When PAPI was in excess, the excess isocyanate group may react with moisture in air or self-polymerize to produce CO_2, thus the high foaming speed resulted in unsatisfied distribution.

Figure 3 shows the SEM images of PIFSs with different 3,4′-ODA contents. Their cell sizes are seen in Table I. Compared to the cell morphology of PIFS-3, it is indicated that the introduction of 3,4′-ODA increases the average cell size of PIFSs. Further, the average cell size increases firstly, and then reduces with increasing 3,4′-ODA. As for PIFS-3-1 and PIFS-3-2, the cells are obvious, namely cell walls were typically distributed with areas of polymer resin. Rather, PIFS-3-3 and PIF-3–4 exhibited a structure where cells are getting indistinct and all in a jumble. The reasons can be explained as follows: the more 3,4′-ODA

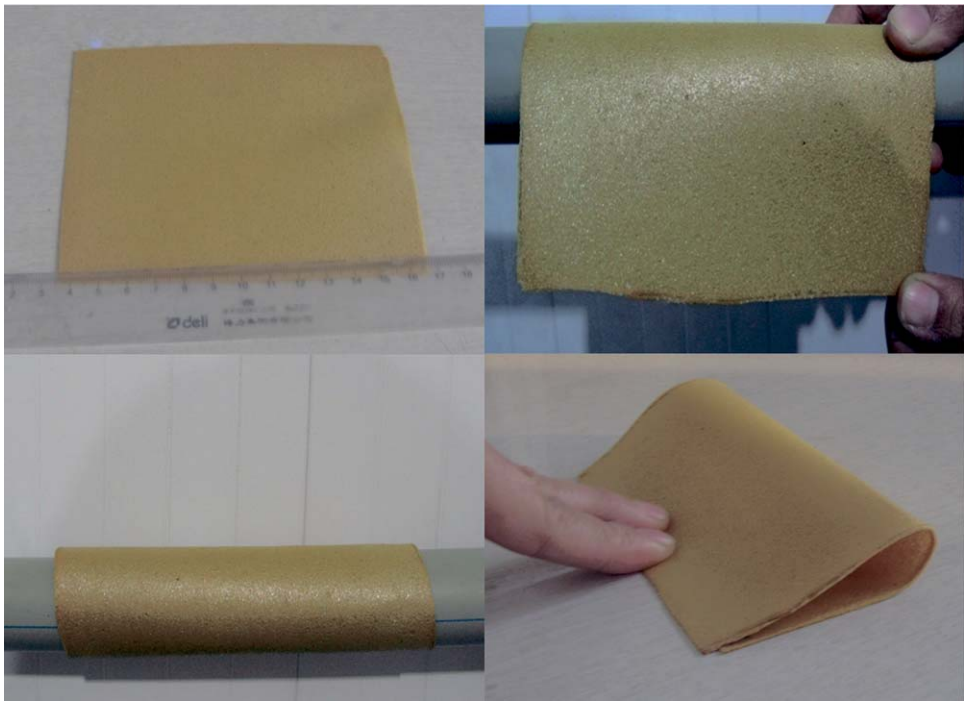

Figure 1. Images of the foam sheets from different angles. [Color figure can be viewed in the online issue, which is available at wileyonlinelibrary.com.]

was used, the less unreacted BTDA was left, leading to more PAPI left, thus the increased amount of CO_2 resulted in larger cells. When the content of 3,4′-ODA increased to a certain extent, the high viscosity of first solution would hinder cell growth during foaming, leading to smaller cell diameter. Further, it can also give rise to inhomogeneous mixing between PAPI and first solution, leading to irregular cell distribution and more collapsing cells.

Figure 4 shows the cell morphologies of front surface and cross section for PIFS-3. As indicated in Figure 4(a) with magnification of ×50, the cells of front surface are almost hexagonal and cell walls are clearly observed. A higher magnification of ×100 [Figure 4(b)] shows that the irregular open cells that are directly adjacent to one another exist below the cell membranes and the cell size is nearly 150 μm with average cellular wall thickness of 30 μm. As shown in Figure 4(c), the cells of cross section exhibit a slightly elliptical morphology due to the compression, and they have average longitudinal dimension of 190 μm and lateral dimension of 50 μm. Comprehensive analysis shows that PIFSs exhibit a structure that front surface displays closed cells made of damaged cell walls and membranes, while internal cells are open, and elliptic vacancies are flatted in the thickness direction from the cross section.

Table I. The Cell Sizes of PIFSs in the Study

Samples	Maximum cell size (μm)	Minimum cell size (μm)	Average cell size (μm)
PIFS-1	216.24	40.23	100.42
PIFS-2	358.09	94.25	150.95
PIFS-3	343.42	167.43	214.50
PIFS-4	449.40	130.10	228.50
PIFS-5	582.11	213.40	339.07
PIFS-3-1	409.54	141.51	250.98
PIFS-3-2	465.53	121.05	267.26
PIFS-3-3	465.65	182.17	290.33
PIFS-3-4	482.75	70.86	242.01

Apparent Density Characterization of PIFSs

Table II presents the apparent densities of PIFSs with different composition. As indicated in Table II, these PIFSs have lower densities ranging from 0.087 g/cm^3 to 0.239 g/cm^3, in contrast to 0.5 mm polyimide aerogel films[15–18] with densities of 0.108–0.451 g/cm^3 fabricated by NASA. As for PIFSs without 3,4′-ODA, the density reduces firstly, and then increases with increasing PAPI content. This could be attributed to the fact that the cells got larger with increasing PAPI content. While in PIFS-5, the collapse degree of cells increased after compression on one hand. And it has lower matrix resin content due to larger cells on the other. For both reasons, its density is only slightly higher than that of PIFS-4. As for samples containing 3,4′-ODA, it is surprising to observe that these samples have densities of 0.087–0.116 g/cm^3, which are further lower than that of samples without 3,4′-ODA. This could be explained as follows: its matrix resin content was lower for intermediate foam with same thickness due to larger cells. On the other hand, linear thermoplastic structure produced by reaction of

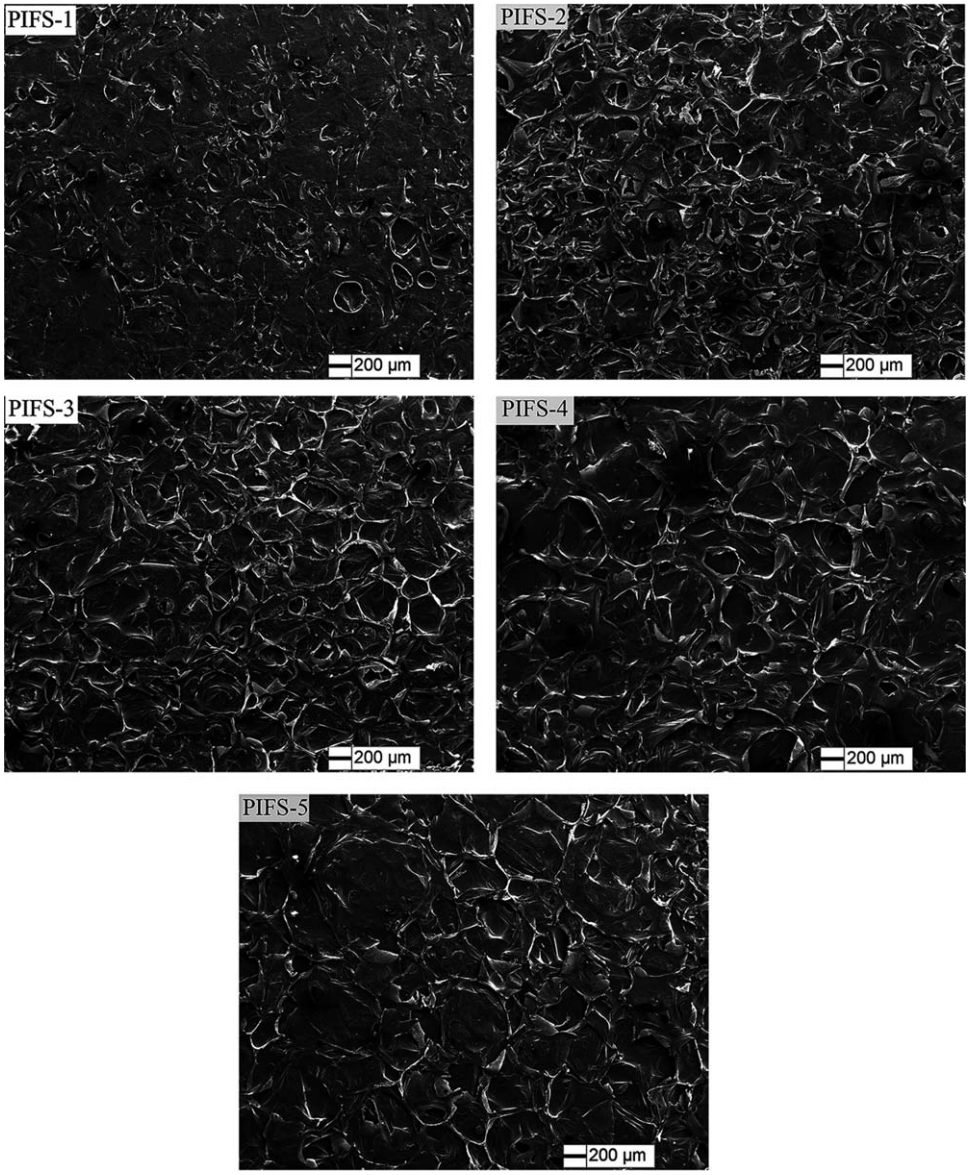

Figure 2. SEM images of PIFSs with different PAPI contents.

BTDA and 3,4′-ODA can move vigorously at high temperature during compression molding, which made the foam have a tendency to expand and resist the pressure, leading to larger volume. In addition, when the mole ratio of 3,4′-ODA to BTDA increases from 0.05 to 0.15, the densities are comparable. However, the density increases to 0.116 g/cm^3 for 3,4′-ODA loading of 20 mol%. According to the analysis above, the high viscosity of first solution for PIFS-3–4 would hinder cell growth during foaming, leading to smaller average cell diameter, thus its matrix resin content was higher. In addition, the high viscosity can also give rise to inhomogeneous mixing between PAPI and first solution, leading to unsatisfied cell distribution and more collapsing cells. For both reasons, the density increased.

As for samples with same composition, the density presents an increasing trend with increasing molding pressure. This may be explained as follows: as the molding pressure increased, more multilayer cells overlapped and its collapse degree increased, resulting in the increasing of density.

Tensile Properties of PIFSs

Tensile properties were measured to verify the structural integrity in order to address the properties such as density and cell structure. The testing features of PIFSs before and after tensile test were shown in Figure 5(a). Figure 5(b,c) show tensile stress-strain curves of PIFSs obtained in our tensile experiments. The tensile toughness (the energy to fracture per volume) was calculated by integrating the area under the stress-strain curve. The tensile stress, elongation at break and tensile toughness are summarized in Table III.

As indicated in Figure 5(b,c), two stages are observed during tensile test. The first stage is characterized by linear elastic region, where tensile stress increases linearly with the strain.

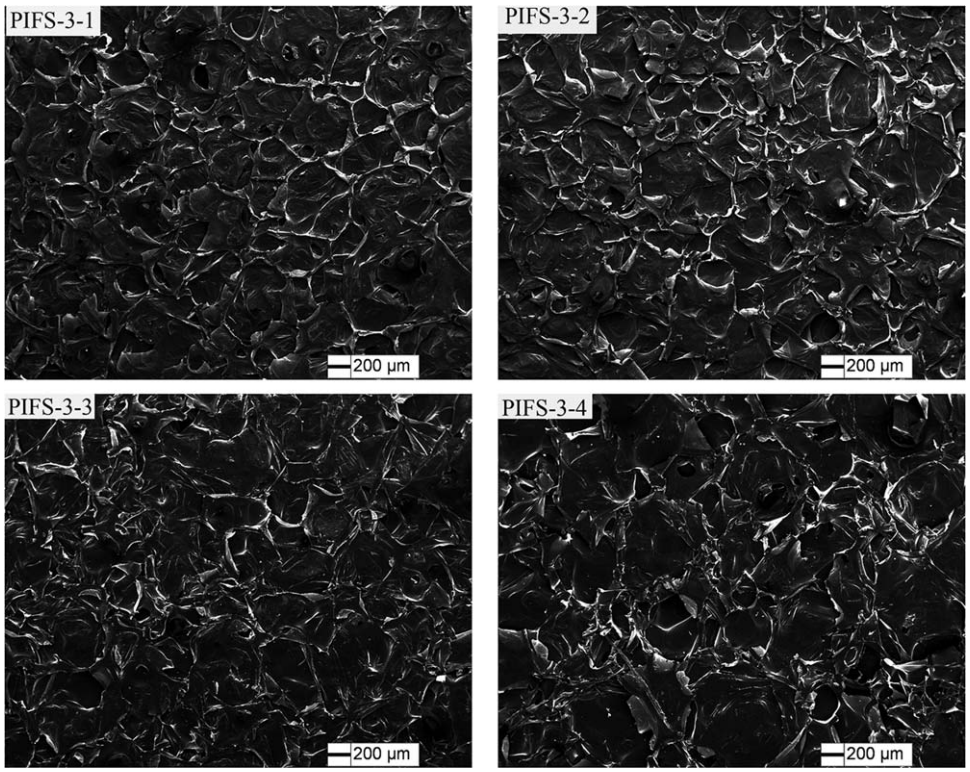

Figure 3. SEM images of PIFSs with different contents of 3, 4'-ODA.

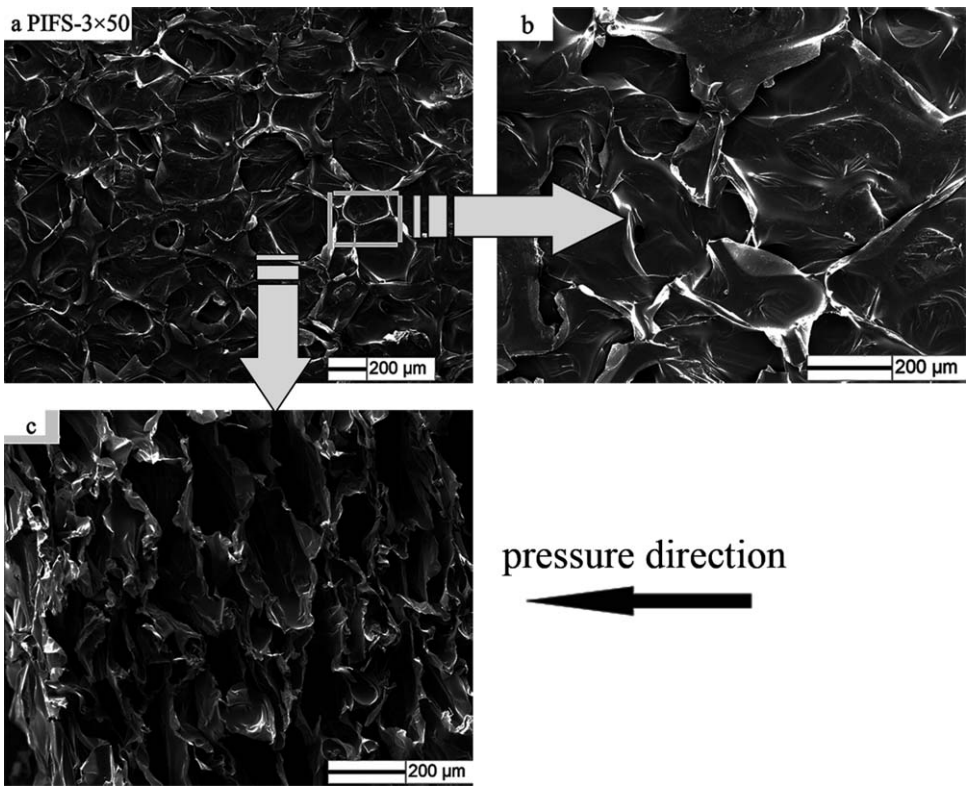

Figure 4. SEM micrographs of PIFS-3. (a, b) front surface, (c) cross section

Table II. Apparent Densities of PIFSs in the Study

Samples	Weight ratio of PAPI to first solution	Mole ratio of 3,4′-ODA to BTDA	Molding pressure (KPa)	Apparent density ($g \bullet cm^{-3}$)
PIFS-1	0.5	0	15.32	0.207 ± 0.010
PIFS-2	0.65	0	15.32	0.168 ± 0.008
PIFS-3	0.8	0	15.32	0.147 ± 0.007
PIFS-3-1′	0.8	0	13.28	0.103 ± 0.005
PIFS-3-2′	0.8	0	18.23	0.180 ± 0.010
PIFS-3-3′	0.8	0	19.76	0.239 ± 0.012
PIFS-4	0.95	0	15.32	0.116 ± 0.006
PIFS-5	1.1	0	15.32	0.129 ± 0.006
PIFS-3-1	0.8	5/100	15.32	0.092 ± 0.015
PIFS-3-2	0.8	10/100	15.32	0.089 ± 0.007
PIFS-3-3	0.8	15/100	15.32	0.087 ± 0.006
PIFS-3-4	0.8	20/100	15.32	0.116 ± 0.012
P1	0.8	20/100	15.32	0.116 ± 0.012
P2	0.8	20/100	18.23	0.152 ± 0.008
P3	0.8	20/100	19.76	0.178 ± 0.009

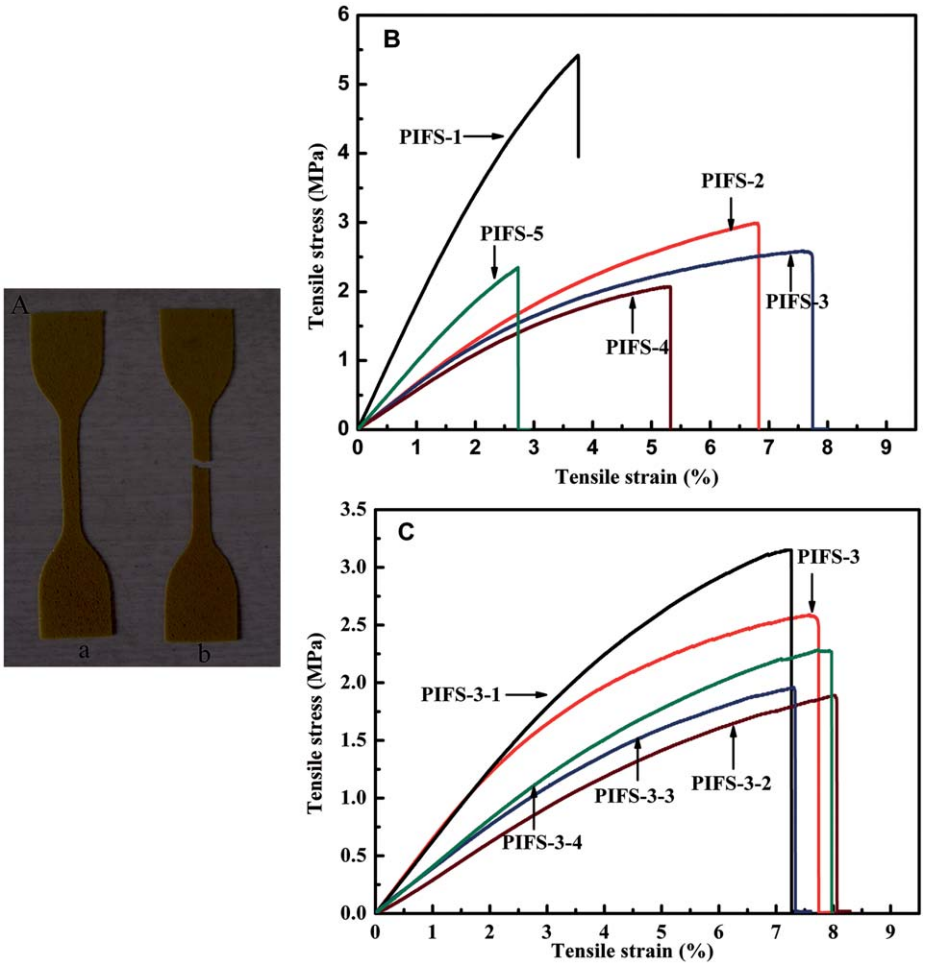

Figure 5. (a) The testing features of PIFSs before and after the tensile test, tensile stress-strain curves of PIFSs with (b) different PAPI contents, and (c) different contents of 3,4′-ODA. [Color figure can be viewed in the online issue, which is available at wileyonlinelibrary.com.]

Table III. Tensile Properties of PIFSs in the Study

Sample	Tensile strength (MPa)	Elongation at break (%)	Tensile toughness ($\times 10^{-2}$)(J/cm^3)
PIFS-1	5.42 ± 0.4	3.75 ± 0.2	11.48 ± 0.8
PIFS-2	2.99 ± 0.1	7.10 ± 0.5	12.39 ± 1
PIFS-3	2.59 ± 0.3	7.76 ± 1	13.28 ± 0.9
PIFS-3-1′	2.26 ± 0.2	6.96 ± 0.1	10.42 ± 0.9
PIFS-3-2′	2.74 ± 0.3	6.60 ± 0.6	11.67 ± 1
PIFS-3-3′	3.15 ± 0.4	6.04 ± 0.4	12.02 ± 1
PIFS-4	2.07 ± 0.4	5.30 ± 0.4	6.69 ± 0.5
PIFS-5	2.35 ± 0.5	2.80 ± 0.2	3.46 ± 0.2
PIFS-3-1	3.15 ± 0.2	7.05 ± 1	13.87 ± 2
PIFS-3-2	1.89 ± 0.2	8.03 ± 0.3	8.50 ± 1
PIFS-3-3	1.96 ± 0.6	7.31 ± 0.2	8.65 ± 0.4
PIFS-3-4	2.33 ± 0.45	7.08 ± 0.8	10.98 ± 0.8

The second stage is characterized by stress relaxation following the rapid brittle fracture. Tensile behaviors of PIFSs are likely best explained by a discussion on the fracture mechanics of polymer foam. Before tension stretching, the cells showed nearly hexagonal morphology. As tensile load was applied, cells were stretched, cell walls were extended and the cells get elongated. When the load increased to a certain extent, fracture of the cell walls occurred, thus brittle failure occurred through the sample, in which the elongation of samples was low.

Another important insight from Figure 5(b) is that the tensile stress of samples without 3,4′-ODA reduces from 5.42 MPa at 0.5 weight ratio of PAPI to first solution to 2.07 MPa at 0.95 weight ratio of PAPI to first solution, and then increases slightly with the increase in PAPI loading, which is consistent with concomitant change in density. It is well known that the mechanical properties of foams are affected by foam density, cell size, cell uniformity, the thickness of cell walls, molecular structure of matrix, and so on. As PAPI increased, cells got larger, and rigid benzene ring density in matrix reduced leading to reducing molecular interactions, and cell walls are thinner, so the tensile strength reduced. When PAPI increased to a certain extent, rigid benzene ring density in matrix increased slightly, thus the results above occurred. PIFS-3 presents the best toughness for which is 1.1–4 times tougher than others due to the relatively uniform distribution of cells and few flaws in sample which are resistant to rupture and favorable for the improvement of toughness.

As indicated in Figure 5(c), PIFS-3-1 exhibits optimal tensile stress of 3.15 MPa which has a 21.6% increment compared to PIFS-3, leading to a 4.4% increment in tensile toughness from 13.28×10^{-2} J/cm^3 to 13.87×10^{-2} J/cm^3. It indicates that the introduction of specific 3,4′-ODA loading can improve the tensile strength and toughness of samples due to stable cells and linear thermoplastic structure. Further, polyamide acid can react with BTDA and PAPI to produce cross-linked structure. However, the foam series of PIFS-3-2–PIFS-3–4 presents comparable tensile stress and toughness which are lower than that of PIFS-3. With the further increase of 3,4′-ODA, the amount of thermoplastic segment structure increased, resulting in reducing amount of crosslink points, thus the rigidity of matrix reduced.

Tensile tests were performed on PIFS-3, PIFS-3-1′, PIFS-3-2′, PIFS-3-3′to verify the relationship between tensile properties and density. As shown in Table III, tensile stress of samples with the same composition presents an increasing trend from 2.26 MPa at 0.103 g/cm^3 to 3.15 MPa at 0.239 g/cm^3 as the density increases due to the increasing of rigid benzene ring density in matrix.

As studied earlier in our research group, polyimide foam had tensile strength of 0.058–0.15 MPa.[25,26] Referring to Table III, the data of the PIFSs at 0.5 mm thickness in this study ranged from 1.89 MPa to 5.42 MPa, which was improved by a factor of 30 times attributed to the increasing density and reducing thickness. Furthermore, previously studied polyimide aerogel films with densities of 0.108–0.451 g/cm^3 at 0.5 mm thickness showed tensile stress of 1.2–4.5 MPa.[16,17] Hence, the prepared PIFSs in our study displayed better tensile property than polyimide aerogel films with similar density.

Thermal Insulation Properties of PIFSs

Because of light weight and high tensile stress, PIFSs could be expected to be the inner material for the MLI in which thermal insulation is an important consideration.[27,28] Thermal conductivity tests of the PIFSs were measured on a thermal conductivity analyzer designed by ourselves previously according to ASTM C 518, which worked well for relatively low thermal conductivity materials. The sample was compressed slightly to minimize the effect of thermal contact resistance. The measurement system was calibrated using one low conductivity reference sample (AC 550) in place of the foam sheets.

The testing principle was based on Fourier's law.[9,29] The heat transfer rate through the flat was calculated using equation as follows:

$$\Phi = \lambda A \frac{\Delta T}{\Delta x} \quad (1)$$

We can develop the equation defining the thermal conductivity

$$\lambda = \frac{\Phi \Delta x}{A \Delta T} \quad (2)$$

where λ is the thermal conductivity, Φ is the heat transfer rate through the sample, A is the area of samples tested along the direction of heat flow, ΔT is the temperature difference between the plates, Δx is the thickness of sample.

As a kind of high performance polymer, PIFSs can be used at both high and low temperature. Samples with different PAPI loading were tested for thermal physical properties between room temperature and 250°C. Figure 6 shows the thermal conductivity of samples versus temperature. As shown in the graph, the thermal conductivity increases significantly with the increment of temperature. This may be ascribed to the fact that thermal motion of the microcosmic molecule increased with the increase of temperature, resulting in an enhancement of heat conduction.

The data of thermal conductivity of PIFSs at 24°C are plotted in Figure 7 to bring out the trends and the important differences as a result of changing the content of PAPI and the content of 3,4′-ODA. As shown in the graph, PIFSs possess low thermal conductivity of 14.37–19.25 mW/m·K, which was about 0.328–0.443 times than that of previously fabricated AC550 with thermal conductivity of 43 mW/m·K at 24°C.[9] This may be explained by way of heat transfer mechanism of polymer foam. Heat transfer in polymeric foams occurs through heat conduction of solid polymer, gas heat conduction, gas heat convection and radiation heat transfer.[29] Compared to AC550 with open cells, partial cells collapsed in PIFSs, which reduced the air heat convection in cells.

From Figure 7(a), we it can be noted that the thermal conductivity increases with the increasing of PAPI at the same temperature due to the variation of cell structures. As PAPI increased, cells became larger. In larger cells where more space of air movement happened, heat convection actually increased, thus the thermal conductivity increased. One interesting insight from Figure 7(b) is the maximum thermal conductivity at 0.10 mole ratio of 3,4′-ODA to BTDA due to the larger cells. Continuing to increase 3,4′-ODA, unsatisfied cell distribution gave rise to the reducing of radiation heat transfer and heat convection, resulting in the thermal conductivity reducing significantly. It seems that the thermal insulation would be improved by the incorporation of specific 3,4′-ODA loading.

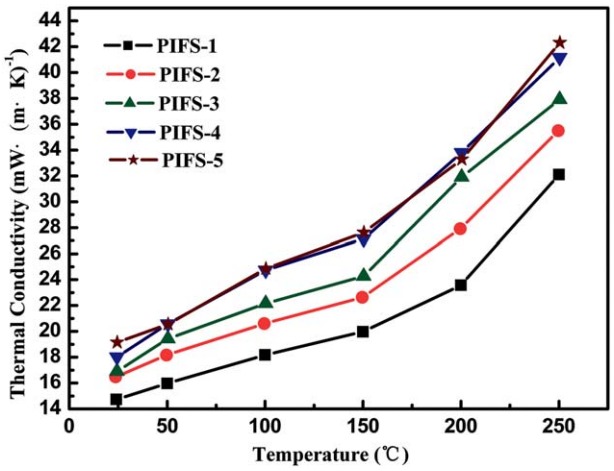

Figure 6. Thermal conductivity of PIFSs with respect to temperature. [Color figure can be viewed in the online issue, which is available at wileyonlinelibrary.com.]

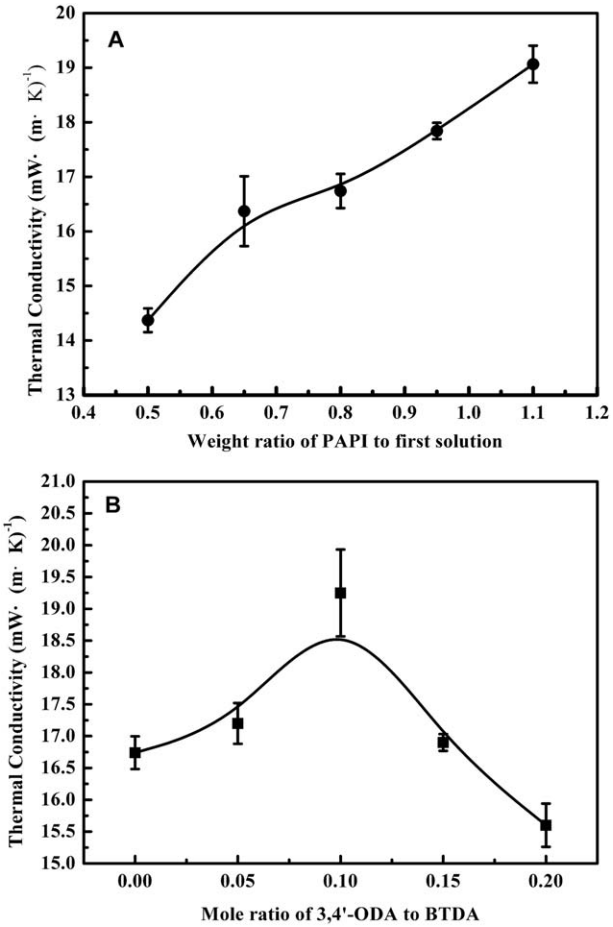

Figure 7. Thermal conductivity of PIFSs with (a) different contents of PAPI and (b) different contents of 3,4′-ODA at 24°C.

Sound Absorption Properties of PIFSs

Sound absorption property must be taken into account for some acoustic applications, including aircraft sidewall treatments.[30,31] It is of interest here to investigate the acoustic behavior of PIFSs which is studied by means of the sound absorption coefficient (α).

The sound absorption coefficients of PIFSs with thickness of 0.5 mm as a function of frequency are presented in Figure 8. As shown in Figure 8(a), at frequencies below 1650 Hz, the α value of samples with different PAPI contents ranges from 0.12 to 0.24 and their variation amplitude is small. This can be attributed to the fact that the sound wavelength is large and the samples are stiff, which make it difficult for sound to penetrate the materials. While the α value increases firstly, and then slightly

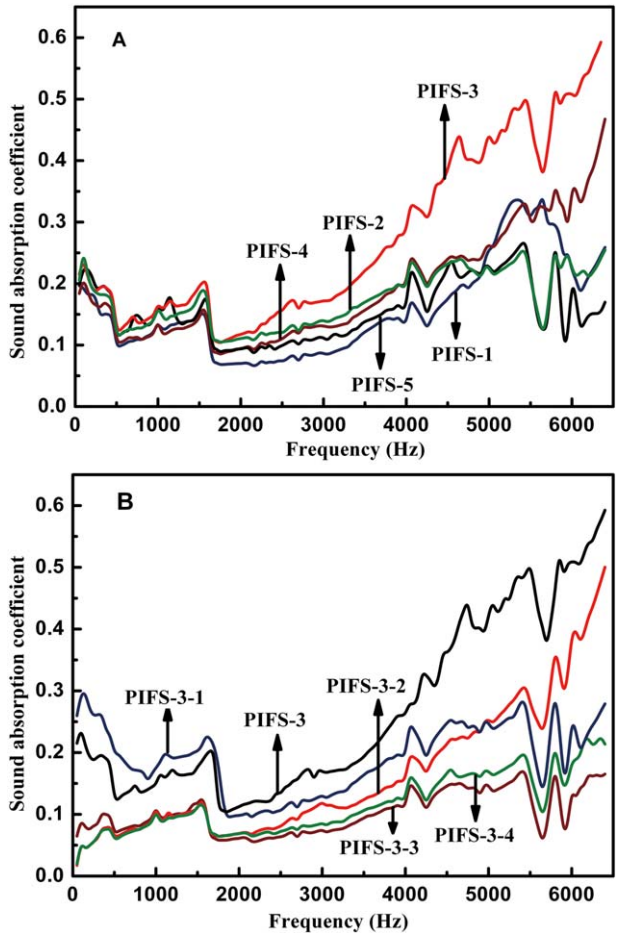

Figure 8. The sound absorption coefficients of PIFSs with (a) different PAPI contents and (b) different 3,4′-ODA contents. [Color figure can be viewed in the online issue, which is available at wileyonlinelibrary.com.]

reduces with increasing PAPI content above 1650 Hz. PIFS-3 is projected to be the optimum level for sound absorption performance on the whole frequency range. It is well known that the sound absorption properties of foams are affected by foam structure and the matrix polymer. As the content of PAPI increased, rigid benzene ring density in matrix reduced and the toughness of polymer chain increased, and the uniformity of cell distribution got better, which made the viscosity dissipation of sound wave increase. When PAPI increased to a certain extent, rigid benzene ring density in matrix increased and the toughness of polymer chain reduced slightly, and the uniformity of cell distribution got worse, thus the α value slightly reduced. PIFS-3 exhibited optimum polymer chain toughness and uniform cell distribution, thus the interfacial reflection of between air and matrix and the intermolecular friction of air molecules as well as the intermolecular friction of matrix polymer chains were enhanced, which made the viscosity dissipation of sound wave increase. As shown in Figure 8(b), PIFS-3-1 out performs the other samples in the frequency band 50–1650 Hz, which indicates that a certain content of 3,4′-ODA allows an improvement of the sound absorption of PIFSs with increase between 0.04 and 0.16 possibly due to linear thermoplastic structure in polymer matrix for which the viscosity dissipation of sound wave increased. However, the addition of 3,4′-ODA was found to reduce the sound absorption coefficients for frequencies above 1650 Hz mainly attributed to the larger cells and ununiform cell distribution. In this case, the viscosity dissipation of sound wave decreased. In addition, the α value of samples reduces firstly, and then increases with the increase of 3,4′-ODA due to the sample-to-sample variations of cell structures. As the cell size increased, and the inter-facial area between the solid frames decreased, leading to the reducing viscosity dissipation of sound wave.

It is well known that the density of samples had some influence on sound absorption property of polyimide foam[32]. In order to investigate the effects, according to the combination of PIFS-3–4, a series of foam sheets with thickness of 0.5 mm varying in density were fabricated by changing the molding pressure. These foam sheets were designated as P1, P2, and P3, respectively. Figure 9 shows the sound absorption coefficients of PIFSs with different densities as a function of frequency. It is shown that in the frequency band 50–1750 Hz, the 0.178 g/cm^3 foam sheet, namely P3, out performs P1 at 0.116 g/cm^3, but both have poorer sound absorption performance than P2 at 0.152 g/cm^3, while the α value increases with increasing density at medium and high frequencies. This can be attributed to the variation of airflow resistance resulting from the variation of density. When density is low, air flow resistance is low, and it is easy for sound to penetrate the sheet, which makes poor acoustic performance. When the density is high enough to result in high air flow resistance, thus it is hard for the sound waves to penetrate the sheet. Hence, porous materials have optimal airflow resistance which is different in different frequency range.

CONCLUSIONS

In summary, we have developed a facile and fast approach for fabrication of lightweight PIFSs with millimeter thickness based on liquid foaming and compression molding technology. The resulting foam sheets varied in cell morphology, density, tensile strength, elongation at break, thermal conductivity, and sound absorption coefficient depending on the content of PAPI and

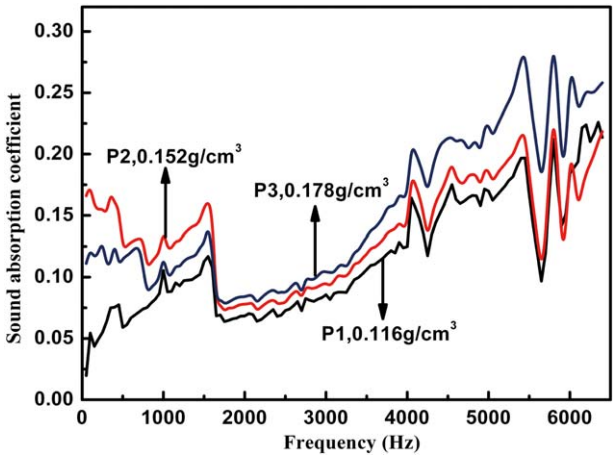

Figure 9. The sound absorption coefficients of PIFSs with different densities. [Color figure can be viewed in the online issue, which is available at wileyonlinelibrary.com.]

the content of 3,4′-ODA. They exhibited a structure that front surface displayed closed cells made of damaged cell walls and membranes, while internal cells were open, and elliptic vacancies were flatted in the thickness direction from cross section. PIFS-3 displayed relatively homogeneous cell morphology. The average cellular diameter increased from 100.42 μm to 339.07 μm with increasing PAPI loading. Also the introduction of 3,4′-ODA increased the average cell size of PIFSs. The PIFSs with thickness of 0.50 mm were flexible and displayed excellent tensile properties and thermal insulation. Furthermore, the apparent density decreased gradually firstly, then increased with increasing PAPI content, while tensile strength presented contrary variation trend. The thermal conductivity increased as the temperature increased as well as at the same temperature with increasing PAPI. Also, the addition of specific 3,4′-ODA content was found to improve the toughness, thermal properties, and sound absorption properties at low frequencies. In addition, the sound absorption coefficients (α) of samples with different PAPI increased and then decreased with increasing PAPI content, and the α increased with increasing density at medium and high frequencies. The well-defined properties potentially make the lightweight PIFSs to be candidates for MLI of spacecrafts. Dielectric properties and other characteristics such as thermal conductivity and sound absorption coefficient for polyimide multilayer are currently under further investigation. Furthermore, optimizing PIFSs to improve the sound absorption coefficient at low frequencies between 50 Hz and 1650 Hz will be also our important work.

REFERENCES

1. Williams, M. K.; Weiser, E. S.; Fesmire, J. E.; Grimsley, B. W.; Smith, T. M.; Brenner, J. R.; Nelson, G. L. *Polym. Adv. Technol.* **2005**, *16*, 167.
2. He, J. M. New Polymeric Foams and Technologies;Chemical Industry Press: Beijing, **2008**.
3. Huang, H. X.; Xu, H. F. *Polym. Adv. Technol.* **2012**, *22*, 822.
4. Kumar, V. *Colloid Surface A* **2005**, *263*, 336.
5. Zhang, H. B.; Yan, Q.; Zheng, W. G.; He, Z. X.; Yu, Z. Z. *ACS Appl. Mater. Interfaces* **2011**, *3*, 918.
6. König, A.; Kroke, E. *Polym. Adv. Technol.* **2011**, *22*, 5.
7. Tay, G. S.; Ong, L. N.; Rozman, H. D. *J. Appl. Polym. Sci.* **2012**, *125*, 158.
8. Moser, M.; Ranzenberger, C.; Lehmann, G. B.; Ritter, H.; Semprimoschnig, C. In proceedings of the 40th International Conference on Environmental Systems, Barcelona, Spain, **2010**.
9. Zhan, M. S.; Wang, K. Polyimide Foam Plastics; National defense industry Press: Beijing, **2010**.
10. Williams, M. K.; Hollanda, D. B.; Melendeza, O.; Weiser, E. S.; Brennerc, J. R.; Nelson, G. L. *Polym. Degrad. Stabil.* **2005**, *88*, 20.
11. Kuwabara, A.; Ozasa, M.; Shimokawa, T.; Watanabe, N.; Nomoto, K. *Adv. Com. Mat.* **2005**, *14*, 343.
12. Tachikawa, S.; Takagi, R.; Mizutani, Y.; Hiasa, Y. Ohnishi, A. In proceedings of the 41st International Conference on Environmental Systems, Oregon, Portland, July 17–21, **2011**.
13. Tachikawa, S.; Mizutani, Y.; Takagi, R. In proceedings of the 9th Asian Thermophysical Properties Conference, Beijing, China, **2010**.
14. Koyashiki, K.; Yamamoto, S. JP Pat. 2011194796(A), **2011**.
15. Meador, M. A.; Malow, E. J.; Silva, R.; Wright, S.; Quade, D.; Vivod, S. L.; Guo, H. Q.; Guo, J.; Cakmak, M. *ACS Appl. Mater. Interfaces* **2012**, *4*, 536.
16. M. A. B.Meador, S.Wright, A.Sandberg, B. N.Nguyen, F. W. V.Keuls, C. H.Mueller, R. R.Solis, F. A.Miranda, *ACS Appl. Mater. Interfaces* **2012**, *4*, 6346.
17. Guo, H. Q.; Meador, M. A.; McCorkle, L.; Quade, D. J.; Guo, J.; Hamilton, B.; Cakmak, M. *ACS Appl. Mater. Interfaces* **2012**, *4*, 5422.
18. Guo, H. Q.; Meador, M. A.; McCorkle, L.; Quade, D. J.; Guo, J.; Hamilton, B.; Cakmak, M.; Sprowl, G. *ACS Appl. Mater. Interfaces* **2011**, *3*, 546.
19. Braun, R. D.; Manning, R. M. *J. Spacer Rockets* **2007**, *44*, 310.
20. Miller, D.; Chatchaisucha, P.; Kumar, V. *Polymer* **2009**, *50*, 5576.
21. Miller, D.; Kumar, V. *Polymer* **2011**, *52*, 2910.
22. Tatsuya, A.; Hiroaki, Y. WO Pat. 2009008499 A1, **2009**.
23. Kaneko, Y.; Yamaguchi, H.; Kohda, M. US Pat. 20110218265A1, **2011**.
24. Koyashiki, K.; Yamamoto, S. JP Pat. 2011218779(A), **2011**.
25. Liu, X.Y.; Zhan, M. S.; Wang, K.; Li, Y.; Bai, Y. F. *Polym. Adv. Technol.* **2012**, *23*, 677.
26. Li, Y.; Liu, X.Y.; Zhan, M. S.; Wang, K. *J. Appl. Polym. Sci.* **2012**, *125*, 4128.
27. Garnier, G. Marouani, S.; Yrieix, B.; Pompeo, C.; Chauvois, M.; Flandin, L.; Brechet, Y. *Polym. Adv. Technol.* **2011**, *22*, 847.
28. Hisasa, Y.; Tahikawa, S.; Ohnishi, A.; Nagasaka, Y. In proceedings of the 18th European on Thermophysical Properties, Pau, France, **2008**.
29. Gibson, L. J.; Ashby, M. F. Cellular Solids: Structure and Properties; Pergamon Press: New York, **1988**.
30. Silcox, R. J.; Cano, R. J.; Howerton, B.; Boloton, J. S. In proceedings of the 51st AIAA Aerospace Science Meeting including the New Horizons and Aerospace Exposition. Grapevine, Texes, January 07–10, **2013**.
31. Doutres, O.; Atalla, N.; Wulliman, R.; Ferguson, S.; Bailey, S. In proceedings of NOISE-CON, Oregon, Portland, July 25–27, **2011**.
32. Liu, X.Y.; Zhan, M. S.; Wang, K. *High Perform. Polym.* **2012**, *24*, 646.